Journal of Materials Science: Materials in Electronics (2019) 30:7400–7409
https://doi.org/10.1007/s10854-019-01053-1

Investigation of structural, superconducting and mechanical properties of Co/Cu substituted YBCO-358 ceramic composites

O. Ozturk[1,2] · R. A. M. Arebat[1] · A. R. A. Nefrow[1] · F. Bulut[3] · G. Guducu[1] · E. Asikuzun[4] · S. Celik[5]

Received: 3 November 2018 / Accepted: 1 March 2019 / Published online: 21 March 2019

Abstract
In this study, we have examined the structural, superconducting and mechanical properties of $Y_3Ba_5Cu_{8-x}Co_xO_{18-\delta}$ system (x = 0, 0.05, 0.1, 0.15, 0.2 and 0.5), which is produced by conventional solid-state reaction method. Produced samples have been examined using X-ray diffraction (XRD), Scanning electron microscopy (SEM), Energy dispersive X-ray spectroscopy (EDS), Vicker's hardness (H_v) and electrical resistance measurement (R–T). According to the XRD patterns, we have obtained that the Co nanopowder doping has been caused some changes on the average grain size, characteristic peak intensities and lattice parameters of the $Y_3Ba_5Cu_8O_{18-\delta}$ crystal system. Furthermore, according to the electrical resistance measurements, the critical temperature (T_c) values of all the samples have tended to decrease constantly with the increment in the doping ratio in the Y358 crystal structure. As for the variation in the microhardness parameters of superconducting materials, the H_v parameters and other related computations (Young's modulus and yield strengths) have been found to increase regularly with the Co/Cu substitution level. Besides, the characteristic H_v curves have confirmed that the whole bulk of Bi-2212 samples showed untypical reverse indentation size effect (RISE) behavior.

1 Introduction

Numerous researches have been conducted on the technological applications of high-T_c superconductors (HTCs) such as Maglev train, trapped flux magnet, flywheel energy storage and magnetic bearing [1–4], since the high temperature superconductor YBaCuO (YBCO) has been discovered. Therefore, many techniques have been used to improve the physical, electrical, microstructural, superconducting and mechanical properties of the HTCs to make them appropriate for applications. In recent years, chemical doping or substitution and changing the production parameters such as the atmosphere, duration, temperature which affecting the result has been studied frequently [5, 6]. As it is well known, the critical temperature of YBCO is one of the most substantial superconducting features in terms of technological applications [7].

With the discovery of $YBa_2Cu_3O_{7-\delta}$ (Y123) bulk superconductor with critical temperature of 92 K, many scientists have started to work on material due to its wide-scale applications [8–10].

In 2009, Aliabadi et al. [11]. reported a new member of YBCO family, which is synthesized by solid state reaction method and has T_c value above 100 K. Higher T_c values of YBCO system have excited the attention of many researchers. The $Y_3Ba_5Cu_{8-x}Co_xO_{18-\delta}$ (Y358) phase discovered contains the CuO chains and CuO_2 planes as in the other members of YBCO family.

In high temperature superconductors, the number of CuO layers and CuO chains plays an important role in critical temperature and superconductivity mechanism. While Y123 phase has two CuO_2 planes and one CuO chain, there are five CuO_2 planes which are separated from two BaO layers and three CuO chains in Y358 phase [12]. According to the previous works, it can be said that the number of CuO_2

✉ O. Ozturk
oozturk@kastamonu.edu.tr

1 Engineering and Architecture Faculty, Department of Electrical and Electronics Engineering, Kastamonu University, 37100 Kastamonu, Turkey

2 Research and Application Center, Kastamonu University, 37100 Kastamonu, Turkey

3 Sinop University, Scientific and Technological Research Applications and Research Center, 57000 Sinop, Turkey

4 Engineering and Architecture Faculty, Department of Metallurgy and Materials Engineering, Kastamonu University, 37100 Kastamonu, Turkey

5 Engineering and Architecture Faculty, Department of Energy Systems Engineering, Sinop University, 57000 Sinop, Turkey

layers and the positions of CuO chains have favorable effect on the critical temperature values of YBCO systems [13]. In addition to these, many groups have been published many papers about Y358 phase [14–20].

In the Cu-doped Y358 system which is studied by T. Metin et al. [21], the critical temperature of the pure sample has been found as 95.6 K. There are some other groups that have studied on Y358 and they have reported the critical temperature value as 94 K [22] and 92.7 K [23] for Y358 phase produced by solid state reaction method. Ekicibil et al. [24]. have been investigated the superconducting properties of Y358 with and without Ca doping. They have been reported that zero resistivity temperature of the undoped Y358 and Ca doped is 87.6 K and 79.4 K respectively. Also in their study Akyol et al. [25]. have been reported the offset temperature of the Y358 as 87.6 K.

In different studies, despite similar critical temperature values were obtained, these results remained below the values obtained by Aliabadi et al. [11]. Also it has been reported that, a and b crystal lattice parameters of Y358 are close to Y123 but c parameter is nearly 3 times bigger than Y123 [11, 12, 26–28]. The crystal structure of Y358 is similar to Y123, except c lattice parameter which is three times bigger than Y123.

Hardness, elastic modulus and yield strength properties of the samples are important as well as the superconducting properties of ceramic superconductors for industrial applications such as fabrication of superconducting wires [29–31]. Microhardness is a mechanical property that measures material resistance by applying deformation technique in a controlled manner. The most common procedure of microhardness determination is Vickers microhardness method [32, 33]. Many papers have been published by researches for investigating Vickers microhardness values of HTCs [34–36].

In this study, $Y_3Ba_5Cu_{8-x}Co_xO_{18-\delta}$ system (x = 0, 0.05, 0.1, 0.15, 0.2 and 0.5) were produced by solid state reaction method and the superconducting, structural and mechanical properties of the samples were investigated by XRD, SEM, EDS, microhardness and resistance (R–T) measurements.

2 Experimental procedure

All the samples synthesized successfully by using solid-state reaction method. In order to reach intended stoichiometries, required amounts of Y_2O_3 (Yttrium (III) oxide %99.99, Alfa Aesar), $BaCO_3$ (Barium carbonate %99.95, Alfa Aesar), CuO (Copper (II) oxide %99.9995, Alfa Aesar) and Co-nanopowder (Cobalt powder-325 mesh %99.5, Alfa Aesar) are weighed depending on the $Y_3Ba_5Cu_{8-x}Co_xO_{18-\delta}$ system ($0 \le x \le 0.5$). The calculated and weighed amounts of powders are grinded in an agate mortar for 1 h. Obtained powders are calcined in furnace with alumina crucible for 24 h at 850 °C, in air atmosphere. After first calcination, powders are grinded again for 1 h and this cycle repeated two times more (in total three calcination processes were applied). Once the third calcination process has been finished, the powders are pressed at 8 tones for 10 min by hydraulics press to obtain bulk samples which have 13 mm diameter and ≈2 mm thickness. Samples in the bulk form are annealed in tube furnace at 930 °C for 24 h in air and cooled down to 500 °C (5 °C/min heating and cooling rates) and sintered for 5 h in O_2 atmosphere. Sintering is one of the most important process for superconductors to obtain denser samples with reduced pore size. Produced samples are named as Y358-0, Y358-5, Y358-10, Y358-15, Y358-20 and Y358-50 according to doping ratios of x = 0.00, 0.05, 0.10, 0.15, 0.20 and 0.50, respectively.

XRD measurements are performed by Bruker D8 advance X-Ray diffractometer with CuKα target with wavelength 1.5418 Å. The Rietveld refinement have used to calculate the impurity phase structure and lattice parameters. SEM and EDS measurements are conducted by FEI Quanta Feg 250 scanning electron microscope to identify grains and surface morphology. Vicker's Microhardness measurements are performed by Shimadzu HMV-2 Vicker's Microhardness Tester and electrical resistance (R–T) measurements are done by standard four probe method by using Janis CCS450 cryostat, Keithley 6221 current source and Keithley 2182A nanovoltmeter.

3 Results and discussion

3.1 XRD measurements

XRD patterns of the samples are obtained between 3–90° at room temperature (Fig. 1). The diffraction patterns of the superconducting systems are used to determine the phase analysis, crystalline size, interplanar distance, cell parameters and texture analyses.

Characteristic peaks in related with the Y358 phase are marked on the patterns and (108) and (018) peaks are given in Fig. 2. Except for the Y358-50 compound, the characteristic peak intensities generally decreased with increasing the doping ratio of Co nanoparticle. The increment in the Co concentration leads to distort Y358 crystal structure. Increased particle growth and the orienting of the particles in the entity of Co ions may be the reason for the decrease in peak intensity. Extra peak related to the Co has not been observed in XRD results. This result can be explained by successful substitution of Co ions with Cu ions of host YBCO superconductor without altering crystal structure. Crystal lattice parameters *a, b* and *c* are calculated by using the XRD data (Eq. 1). The obtained a and b values are

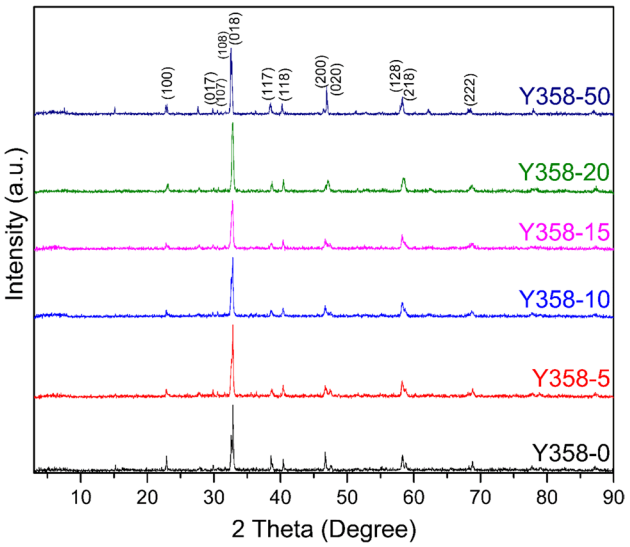

Fig. 1 XRD patterns of produced samples

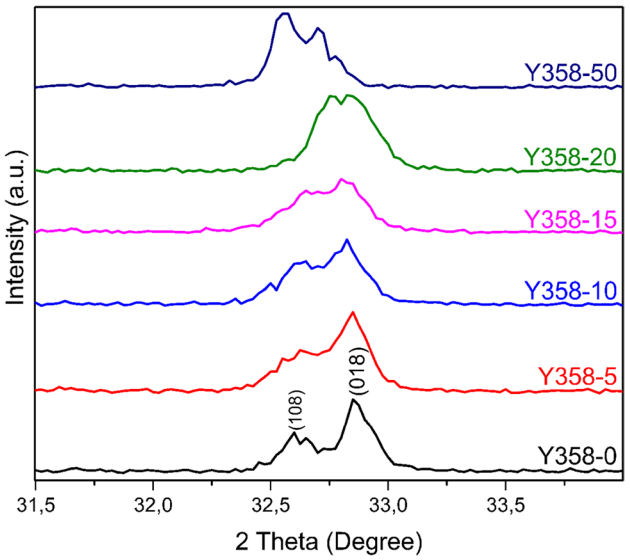

Fig. 2 (108) and (018) peaks that are distinctive for Y358 phase

found to be close to each other, but an enlargement in the *c*-axis length with increasing Co ratio. The change in the *a, b, c* lattice constant parameters did not completely disrupt the orthorhombic structure but little shifts from the ideal orthorhombic structure were observed. While the *a* and *b* lattice cell parameters are nearly the same with Y123 superconducting phase, the *c*-axis values of Y358 are noted to be nearly 3 times of Y123 [12, 13, 37].

$$\frac{1}{d^2} = \frac{h^2}{a^2} + \frac{k^2}{b^2} + \frac{l^2}{c^2} \tag{1}$$

Grain size value determined from the X-Ray diffraction patterns is one of the most important characteristics for the engineering, industrial and technological applications of the superconducting materials. The value can be calculated by means of the well-known approach, the Warren-Sherrer equation (Eq. 2 and Eq. 3). The average grain sizes estimated from FWHM (full width half maximum) data in XRD spectrum are calculated using four peaks in spectrum (018), (017), (100) and (117) [38]. The average grain size parameter has been found to change in a range of 22.46 nm (for the bulk Y358-0 compound)–31.47 nm (for the Y358-50 superconducting material). Thus, Table 1 guarantees that the average crystallite size of produced samples increases constantly with enhancing the doping ratio of Co nanoparticle in the Y358 crystal system. The change in the average grain size may be related to the bonding states of Cu and Co elements. In more detail, the difference between the configurations of outer-shell electrons for the Cu and Co elements can affect the dominant role on the grain size parameters. The representative configuration for the copper element is 3d10 4s1 when 3d7 4s2 is known the outer-shell electrons for the cobalt element. In this respect, the cobalt atoms are much easier to bond with surrounding oxygen atoms by d–s–p orbital hybridization as compared to the copper atoms when surrounding the oxygen atoms in the crystal structure. Thus, the formation of bond between the Cu and oxygen atoms requires much more energy than that of Co atoms [39, 40]. The more extra energy the formation of bond needs the

Table 1 Orthorhombicity and lattice parameters calculated by XRD and Reitveld refinement data

Sample	Grain Size (nm)	Calculated from XRD			Reitveld refinement									δ
					Y358 phase			Y123 phase			G.O.F	Rw	Rwp	
		a (Å)	b (Å)	c (Å)	a (Å)	b (Å)	c (Å)	a (Å)	b (Å)	c (Å)				
Y358-0	22.46	3.88	3.82	31.04	3.83	3.88	30.93	3.47	3.88	11.64	0.41	9.19	12.75	0.843
Y358-5	23.32	3.88	3.82	31.01	3.84	3.90	31.07	3.83	3.88	11.68	0.38	7.67	11.48	0.820
Y358-10	23.37	3.88	3.82	31.00	3.84	3.88	30.88	3.83	3.89	11.62	0.34	7.52	10.51	0.810
Y358-15	24.02	3.89	3.82	30.97	3.85	3.89	31.10	3.83	3.87	11.67	0.34	7.67	10.23	0.791
Y358-20	30.41	3.89	3.83	30.93	3.84	3.89	30.97	3.84	3.86	11.66	0.33	6.96	9.54	0.787
Y358-50	31.47	3.90	3.86	30.87	3.84	3.89	30.96	3.84	3.87	11.68	0.42	9.05	12.41	0.516

shorter average grain size the material obtains. Namely, the impact of bonding formed by the Cu and O atoms presents the dominant character in the crystal matrix. Consequently, the grain size tends to increase systematically with the augmentation in the cobalt impurity level in the YBCO-358 superconducting crystal structure.

$$D = \frac{0.9\lambda}{B\cos\theta} \tag{2}$$

$$B^2 = B_s^2 - B_m^2 \tag{3}$$

The calculated, measured XRD patterns of the Y358-0 sample and their difference are given in Fig. 3. These data were obtained by applying Rietveld refinement with Janna 2006 program. It was observed that the samples produced had Y358 and Y123 phases respectively in Pmm2 and Pmmm space groups. For the Y358 structure, the lattice parameters obtained from refinement process are given in Table 1 together with the calculated XRD parameters. According to the comparisons in Table 1, it is clear that all samples produced have orthorhombic structure. It is clear that the values obtained are consistent with the literature [11, 12]. Additionally, goodness of fit (G.O.F.) and quality factors (Rp, Rwp) obtained from refinement process are given in Table 1. From the XRD patterns, the values calculated with the Warren Sherrer formula are consistent with the Rietveld refinement values.

The orthorhombicity (δ) of samples has been calculated by using $\delta = 100(a-b)/(a+b)$ relation and results are given in Table 1. From the Table 1, orthorhombicity parameter of the samples decreases with the doping ratio of Co. The Y358-0 sample had 0.8435 orthorhombicity, while the orthorhombicity of Y358-50 sample was 0.5169. This shows that the structure gradually deteriorated with the increasing of doping ratio.

3.2 SEM, EDS measurements

SEM images in the different magnifications taken from the specimen surfaces of undoped and Co doped Y358 bulk samples are shown in Fig. 4a–f. In the SEM images given in Fig. 3, the images on the inner corner have a magnification of 15,000 and a scale of 5 μm, while the external images have a magnification of 5000 and a scale of 20 μm.

When the SEM images are examined, it is seen that the Y358 phase has a layered grain structure known as the plate-like [41]. In the structures, the particles are observed to grow randomly in all the directions. This is due to the fact that two-dimensional growth occurs faster and requires less energy than the grain refinement [42]. As seen from the SEM figures, the surface morphology of produced samples is found to depend extremely on the Co substitution ratio. The particle sizes and distances between particles are changed due to the increment in the doping ratio. Also, the surface porosity is obtained to change by the Co doping level. The increase in particle sizes (seen clearly in SEM images) is consistent with XRD data. According to the SEM images, the homogeneity of the samples prepared is observed to decrease regularly with increasing the Co substitution ratio.

The elements in the material, possible impurities and contribution element rates can quantitatively be obtained by the EDS analysis. The experimental results of EDS analysis are

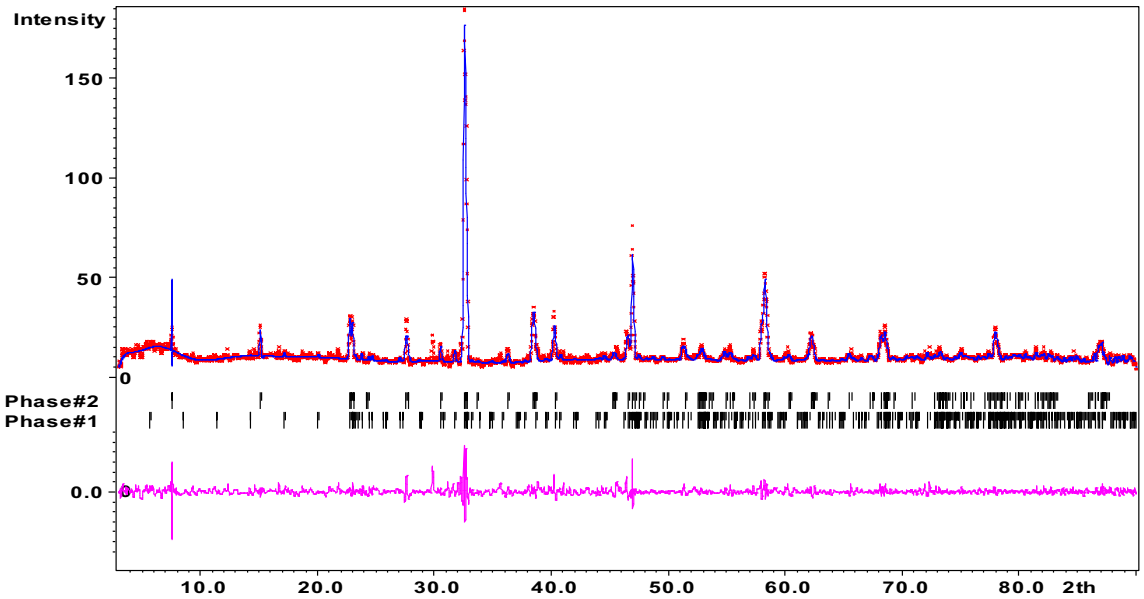

Fig. 3 Results of Reitveld refinemet apllied for Y358-0 sample (Phase1 and Phase2 are Y358 and Y123 phases, respectively)

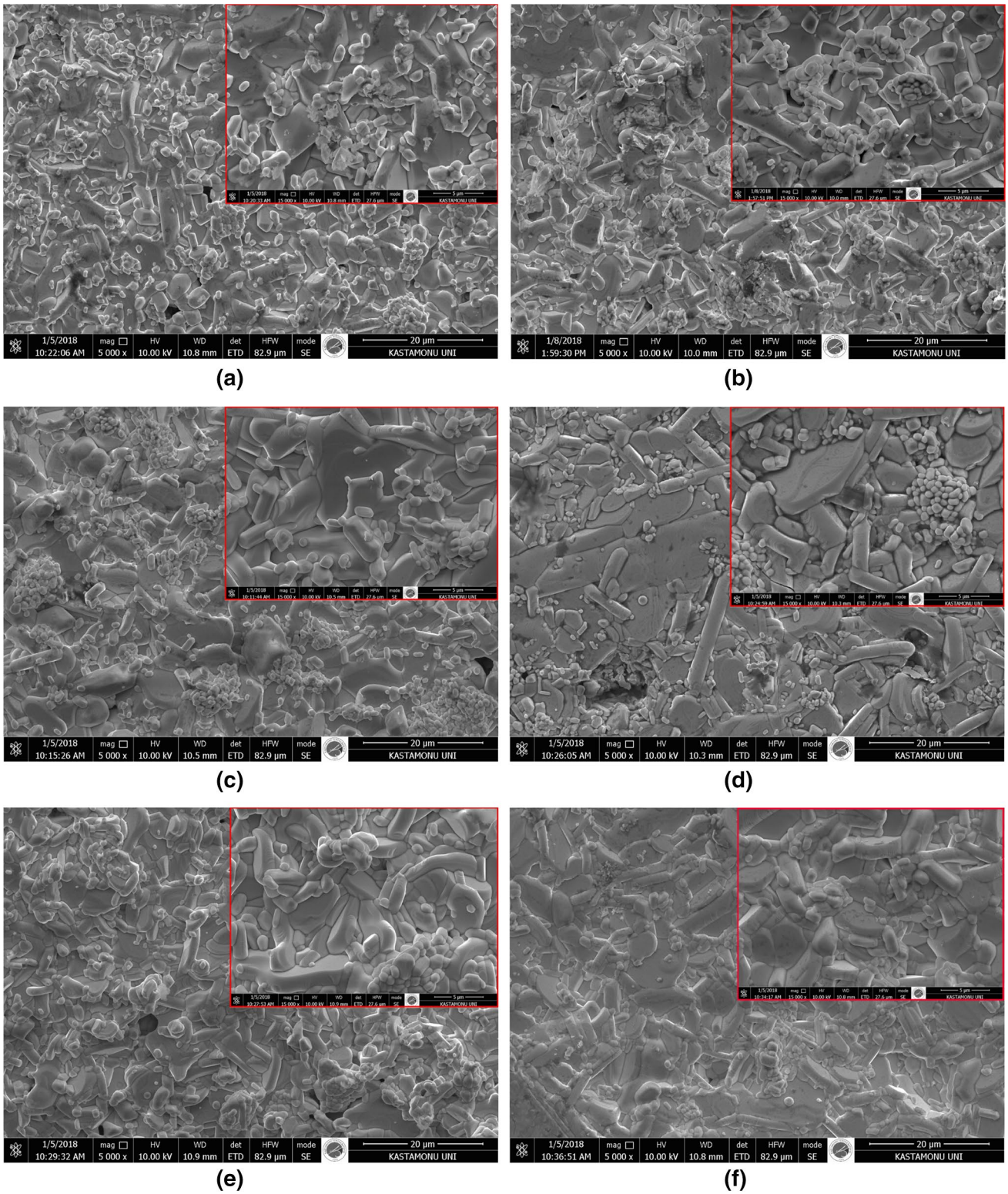

Fig. 4 SEM images of the produced samples **a** Y358-0, **b** Y358-5, **c** Y358-10, **d** Y358-15, **e** Y358-20, **f** Y358-50

given in Fig. 5a–f (In Fig. 5, the X- and Y- axis represents the energy and count respectively). According to the figures, every material prepared in this work consists of the used elements (Y, Ba, Cu, Co and O elements) throughout the preparation process. However, the cobalt element distribution is not detected for the pure sample. This is attributed

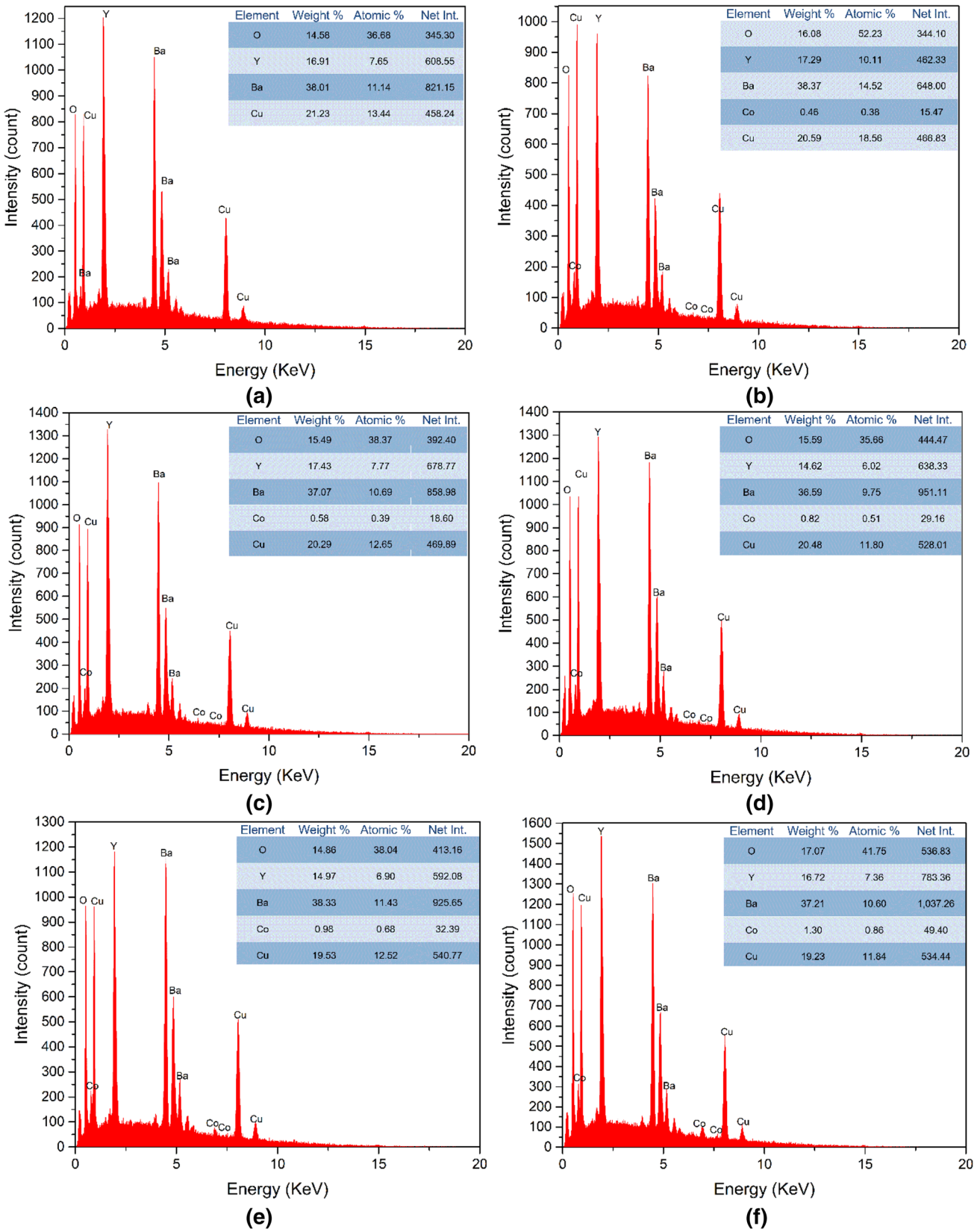

Fig. 5 EDS images and tables of the produced samples **a** Y358-0, **b** Y358-5, **c** Y358-10, **d** Y358-15, **e** Y358-20, **f** Y358-50

to the fact that the preparation process for the bulk YBCO-358 superconducting ceramic composites is performed thoroughly. Moreover, one can see the intensity and related weight percentage values of Y, Ba, Cu, Co and O elements in the tables inside Fig. 5a–f. It is obvious from the figure that the Y, Ba, Cu and O elements exhibit approximately constant for all the pure and Co/Cu substituted YBCO-358 materials whereas the weight percentage value founded on the cobalt element distribution is found to enhance regularly with the increment in the level of Co-nanopowder dopant material in the YBCO-358 crystal structure as planned. At the same time, generally the Cu ratio tends to decrease constantly with increasing the Co element ratio. It is just this last descriptor that is successfully partial substitution of Cu impurities by the Co elements (occupation of Cu-sites in part by Co atoms) in the YBCO-358 superconducting crystal structure [43]. To sum up, the variation of the element distributions displays why the structural, superconducting and mechanical characteristic properties diminish remarkably with the presence of the cobalt impurity in the YBCO-358 superconducting crystal structure.

3.3 Electrical measurements

The electrical resistance of samples produced was measured in the range of 45–300 K. To investigate the effects of Co content in the Y358 system, the dc electrical resistance as a function of temperature (R–T) measurements have been performed and the measurement results were represented in Fig. 6 in detail. Figure 7 is the electrical resistance graph of the Y358-50 sample, which does not show superconducting properties. Standard four probe methods were chosen to measure electrical resistance and 5 mA DC current was applied to the sample surface.

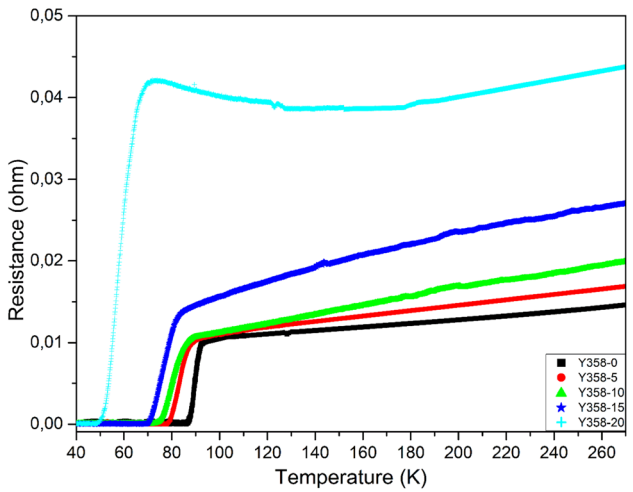

Fig. 6 Resistance as a function of temperature curves for produced samples

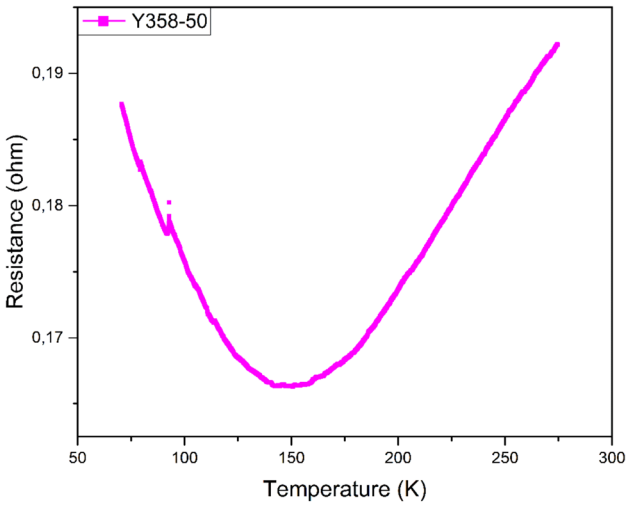

Fig. 7 Resistance dependences on the temperature for Y358-50 sample

The offset (T_c^{offset}) and onset (T_c^{onset}) transition critical temperature values and broadening degrees (ΔT) extracted from the R–T curves are given in Table 2. Above the T_c^{onset} value all samples were found to show metallic-insulator behavior. The room temperature resistance of produced samples increases in proportion to the contribution of Co nanoparticle. The reason of increment in the room temperature resistance values could be due to the increased Co doping ratio in the crystal system.

It is visible from Table 2 that both the T_c^{onset} and T_c^{offset} values decreased consistently with increasing the Co content level in the system. The highest and lowest T_c^{onset} values were observed as 92.42 K and 68.55 K for Y358-0 and Y358-20, respectively. It is clear from the figure that the electrical resistance curves of the produced samples vary with the Co content. The difference between T_c^{onset} and T_c^{offset} is named as transition temperature width (ΔT) and the results are given in Table 2. With the increment in the doping ratio, the transition temperature decreases while the ΔT value enhances. This case is in accordance with the existence of impurities in the Y358 system, weak links between the superconducting grains and grain disorientations, supporting the results of SEM measurements. It can be a result

Table 2 Critical temperature values of superconducting samples

Samples	T_c^{onset} (K)	T_c^{offset} (K)	ΔT_c (K)
Y358-0	92.48	86.20	6.28
Y358-5	88.22	78.24	9.98
Y358-10	85.62	72.84	12.78
Y358-15	83.53	69.81	13.72
Y358-20	68.55	49.02	19.53

of the enhancement in the impurities in the crystal structure [11].

3.4 Mechanical measurements

Microhardness is a test for measuring the hardness and defining the mechanical properties of the materials. Vickers hardness is one of the most common methods used to define the mechanical properties. Vickers hardness values depend on measured the diameters of an indentation which left by a pyramidal indenter tip with different loads. In the present study, five different loads (F = 0.245, 0.490, 0.980, 1.960, 2.940 N) were used to investigate mechanical properties of Y358 samples at room temperature. Vickers microhardness values (H_V) are also calculated using Eq. 4:

$$H_V = 1854.4\left(\frac{F}{\left(\frac{d_1+d_2}{2}\right)^2}\right) \quad (4)$$

where, d_1 and d_2 are the diameters of indentation and F is the applied load. To make more accurate measurements, the microhardness values were determined as the average of measurements taken at 10 different points of sample surface.

The elasticity (E) which named as Young's module in the literature, is the elastic deformation that occurs with the applied force on any material. Young's module is calculated as in Eq. 5. Yield strength (Y) expresses the transition point of elastic deformation to plastic deformation and can be calculated by Eq. 6 [33, 44].

$$E = 81.9635\, H_V \quad (5)$$

$$Y \approx H_V/3 \quad (6)$$

In microhardness characterization, the material behavior can be ISE (indentation size effect) or RISE (reverse indentation size effect) [45, 46]. RISE behavior is defined as the decrement in the hardness by increasing the applied test load, and besides the increment in the hardness by increasing the applied load defined as ISE. Figure 7 shows the variation of the microhardness values depending on the applied loads. Table 3 represents the calculated parameters of the hardness measurement.

According to the combination of Fig. 8 and Table 3, the microhardness values of all samples are found to increase with

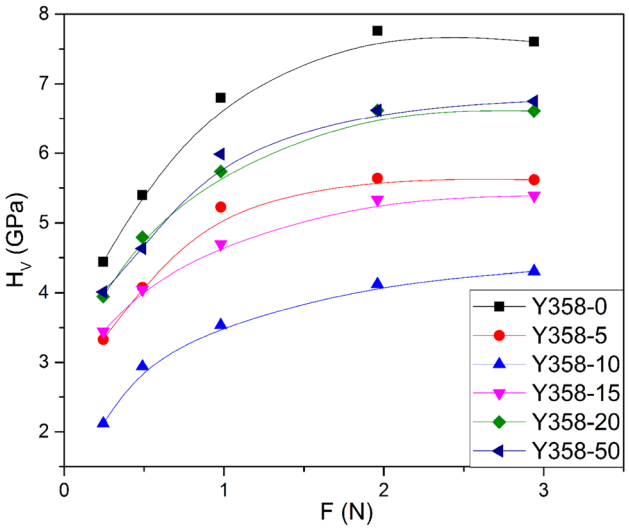

Fig. 8 Variation of load dependent microhardness H_V with applied force F

Table 3 The calculated load dependent H_V, E and Y for the samples

Samples	F (N)	d (nm)	H_V (GPa)	E (GPa)	Y (GPa)	Samples	F (N)	d (nm)	H_V (GPa)	E (GPa)	Y (GPa)
Y358-0	0.245	10.11	4.441	363.964	1.480	Y358-15	0.245	11.48	3.445	282.393	1.148
	0.490	12.97	5.400	442.618	1.800		0.490	14.99	4.046	331.597	1.349
	0.980	16.35	6.800	557.318	2.267		0.980	19.67	4.695	384.788	1.565
	1.960	21.64	7.763	636.256	2.588		1.960	26.11	5.333	437.110	1.778
	2.940	26.77	7.607	623.477	2.536		2.940	31.80	5.391	441.832	1.797
Y358-5	0.245	11.68	3.330	272.963	1.110	Y358-20	0.245	10.73	3.947	323.513	1.316
	0.490	14.93	4.078	334.253	1.359		0.490	13.77	4.795	393.020	1.598
	0.980	18.65	5.226	428.322	1.742		0.980	17.80	5.737	470.253	1.912
	1.960	25.39	5.640	462.241	1.880		1.960	23.43	6.619	542.554	2.206
	2.940	31.15	5.618	460.490	1.873		2.940	28.72	6.611	541.848	2.204
Y358-10	0.245	14.64	2.119	173.654	0.706	Y358-50	0.245	10.64	4.013	328.891	1.338
	0.490	17.58	2.940	240.935	0.980		0.490	14.01	4.632	379.663	1.544
	0.980	22.67	3.535	289.777	1.178		0.980	17.43	5.985	490.562	1.995
	1.960	29.69	4.123	337.899	1.374		1.960	23.43	6.621	542.713	2.207
	2.940	35.59	4.304	352.789	1.435		2.940	28.42	6.751	553.357	2.250

the enhancement in the applied test load, in short all the samples produced in this work show RISE behavior. It shows that the indentation size is related to applied load. The undoped sample, Y358-0, has the highest microhardness value. The microhardness values decreased at the doping ratio of Y358-05 and Y358-10, and then tended to increase. When the elastic modulus and yield strength values given in the table are examined, Y358-0 sample with the highest fracture toughness seems to have the highest elastic modulus at the same time.

4 Conclusion

The superconducting $Y_3Ba_5Cu_{8-x}Co_xO_{18-\delta}$ samples (with x = 0, 0.05, 0.1, 0.15, 0.2 and 0.5) were successfully produced by conventional solid state reaction method. Microstructural, superconducting, mechanical properties of all the samples were investigated by XRD, SEM, EDS, R-T, and Vickers microhardness measurements. The grain size values calculated from the XRD data were found to increase with increasing doping ratio. This is also supported by SEM images. According to the XRD results, the extra peak, which related to the Co impurity is not been observed. This result can be explained by the successful substitution of Co ions with Cu ions of host YBCO superconductor without altering crystal structure. The lattice parameters were calculated from both XRD data and Reitveld refinement. As a result, the lattice cell constants obtained in two ways are compatible with each other and with the literature. In addition, when EDS results are investigated, it can be said that the Cu ratio decreases with the increament in the Co substitution ratio. This result displays that the Co ions are displaced by the Cu ions in the standard crystal structure. It has been observed that the critical temperature values obtained from the dc electrical resistance measurements decrease with increasing the doping ratio. Besides, the values of transition temperature width (ΔT) increased with the increasing doping ratio. The electrical resistance measurements present that the normal state resistance of samples produced increased regularly with increasing the Co substitution ratio. The change of Co ratio in these samples resulted in the change of many parameters; such as room temperature resistance, critical temperature value and critical temperature transition value. It was determined that the hardness behavior of all samples was the reverse indentation size effect (RISE), and also the undoped sample had the highest hardness value, while Y358-10 has the lowest hardness value.

References

1. W. Jiasu, W. Suyu, R. Zhongyou, D. Xiaogang, L. Guobin, L. Jisan, Z. Cuifang, H. Haiyu, D. Changyan, Z. Dequi, IEEE Trans. Appl. Supercond. **9**, 904 (1999)
2. J.R. Hull, Supercond. Sci. Technol. **13**, R1 (2000)
3. R. De Andrade, A.C. Ferreira, G.G. Sotelo, W.I. Suemitsu, L.G.B. Rolim, J.L.S. Neto, M.A. Neves, V.A. Dos Santos, G.C. Da Costa, M. Rosario, R. Stephan, R. Nicolsky, Phys. C Supercond. **408**, 930–931 (2004)
4. G. Krabbes, G. Fuchs, P. Verges, P. Diko, G. Stöver, S. Gruss, Phys. C Supercond. **378**, 636–640 (2002)
5. M. Dogruer, G. Yildirim, E. Yucel, C. Terzioglu, J. Mater. Sci. **23**, 1965 (2012)
6. D. Lee, J. Seo, L. de los Santos Valladares, A.B. Domínguez, A.M. Osorio, Anaya, C.H.W. Barnes, J. Supercond. Novel Magn. **29**, 41 (2016)
7. S. Bolat, S. Kutuk, J. Supercond. Novel Magn. **25**, 731 (2012)
8. P. Marsh, R.M. Fleming, M.L. Mandich, A.M. DeSantolo, J. Kwo, M. Hong, L.J. Martinez-Miranda, Nature **334**, 141 (1988)
9. P.T. Yang, W.M. Yang, Y. Abula, X.Q. Su, L.L. Zhang, Ceram. Int. **43**(3), 3010 (2017)
10. P. Bordet, C. Chaillout, J. Chenavas, J.L. Hodeau, M. Marezio, J. Karpinski, E. Kaldis, Nature **334**, 596 (1988)
11. A. Aliabadi, Y. Akhavan Farshchi, M. Akhavan, Phys. C Supercond. **469**, 2012 (2009)
12. S. Gholipour, V. Daadmehr, A.T. Rezakhani, H. Khosroabadi, F.S. Tehrani, R.H. Akbarnejad, J. Supercond. Novel Magn. **25**, 2253 (2012)
13. U. Topal, M. Akdogan, H. Ozkan, J. Supercond. Novel Magn. **18**, 2099 (2011)
14. Y. Slimani, E. Hannachi, M.K. Ben Salem, A. Hamrita, M. Ben, Salem, F. Ben, Azzouz, Mod. Phys. Lett. B **29**, 1550227 (2015)
15. Y. Slimani, E. Hannachi, A. Hamrita, M.B. Salem, M. Zouaoui, M.B. Salem, F.B. Azzouz, J. Supercond. Novel Magn. **28**, 487 (2015)
16. Y. Slimani, E. Hannachi, M. Zouaoui, F.B. Azzouz, M.B. Salem, J. Supercond. Novel Magn. **31**, 2339 (2018)
17. F.T. Dias, C.P.D. Oliveira, V.D.N. Vieira, D.L. Silva, F. Mesquita, M.L.D. Almeida, J. Schaf, P. Pureur, J. Phys. Conf. Ser. **568**, 22009 (2014)
18. A. Esmaeili, H. Sedghi, M. Amniat-Talab, M. Talebian, Eur. Phys. J. B **79**, 443 (2011)
19. Y. Slimani, E. Hannachi, F.B. Azzouz, M.B. Salem, Cryogenics **92**, 5 (2018)
20. Y. Slimani, E. Hannachi, A. Hamrita, M.B. Salem, F.B. Azzouz, A. Manikandan, M.B. Salem, Ceram. Int. **44**, 19950 (2018)
21. T. Metin, M. Tepe, J. Supercond. Novel Magn. **30**, 1083 (2017)
22. S. Sujinnapram, P. Udomsamuthirun, T. Kruaehong, T. Nilkamjon, S. Ratreng, Bull. Mater. Sci. **34**, 1053 (2011)
23. P. Udomsamuthirun, T. Kruaehong, T. Nilkamjon, S. Ratreng, J. Supercond. Novel Magn. **23**, 1377 (2010)
24. A. Ekicibil, S.K. Cetin, A.O. Ayaş, A. Coşkun, T. Fırat, K. Kıymac, Solid State Sci. **13**, 1954 (2011)
25. M. Akyol, A.O. Ayaş, G. Akça, S.K. Çetin, A. Ekicibil, Bull. Mater. Sci. **38**, 1231 (2015)
26. A.O. Ayaş, A. Ekicibil, S.K. Çetin, A. Coşkun, A.O. Er, Y. Ufuktepe, T. Fırat, K. Kıymaç, J. Supercond. Novel Magn. **24**, 2243 (2011)
27. M.M. Barakat, A.I. Abou-Aly, R. Awad, N.S. Aly, S. Ibrahim, J. Alloys Compd. **652**, 158 (2015)
28. A. Esmaeili, H. Sedghi, M.M. Golzan, M. Amniat-Talab, J. Supercond. Novel Magn. **24**, 2237 (2011)
29. S. Pavan Kumar Naik, M. Santosh, P.M. Swarup, Raju, J. Supercond. Novel Magn. (2017)
30. C. Terzioglu, A. Varilci, I. Belenli, J. Alloys Compd. **478**, 836 (2009)
31. M. Dogruer, G. Yildirim, O. Ozturk, A. Varilci, N. Soylu, O. Gorur, C. Terzioglu, J. Mater. Sci. **24**, 1264 (2013)
32. O. Ozturk, M. Erdem, E. Asikuzun, O. Yildiz, G. Yildirim, A. Varilci, C. Terzioglu, J. Mater. Sci. **24**, 230 (2013)
33. O. Ozturk, J. Mater. Sci. **23**, 1235 (2012)

34. U. Kölemen, S. Çelebi, Y. Yoshino, A. Öztürk, Phys. C Supercond. **406**(1–2), 20 (2004)
35. C. Terzioglu, J. Alloys Compd. **509**, 87 (2011)
36. Y. Yoshino, A. Iwabuchi, K. Noto, N. Sakai, M. Murakami, Phys. C Supercond. **357**, 796–798 (2001)
37. M.S.M. Suan, M.R. Johan, T. Chua, Siang, Phys. C Supercond. **480**, 75 (2012)
38. Y. Slimani, E. Hannachi, M.K. Ben Salem, F. Ben, Azzouz, M. Ben Salem, Appl. Phys. A **124**, 1 (2018)
39. G. Yildirim, M. Dogruer, F. Karaboga, C. Terzioglu, J. Alloys Compd. **584**, 344 (2014)
40. A.T. Ulgen, T. Turgay, C. Terzioglu, G. Yildirim, M. Oz, J. Alloys Compd. **764**, 755 (2018)
41. Y. Slimani, E. Hannachi, F. Ben Azzouz, M. Ben Salem, J. Supercond. Novel Magn. (2018). https://doi.org/10.1007/s10948-018-4746-0
42. Y. Slimani, E. Hannachi, M.K.B. Salem, A. Hamrita, A. Varilci, W. Dachraoui, M.B. Salem, F.B. Azzouz, Physica B **450**, 7–15 (2014)
43. G. Yildirim, J. Alloys Compd. **578**, 526 (2013)
44. E. Asikuzun, J. Supercond. Novel Magn. **31**, 3509 (2018)
45. Y. Zalaoglu, B. Akkurt, M. Oz, G. Yildirim, J. Mater. Sci. **28**, 12839 (2017)
46. B. Akkurt, G. Yildirim, J. Mater. Sci. **27**, 13034 (2016)